Modern Research in Catalysis, 2018, 7, 1-16
http://www.scirp.org/journal/mrc
ISSN Online: 2168-4499
ISSN Print: 2168-4480

# Improvement of a Mesh-Type Cu/Ni/γ-$Al_2O_3$/Al Catalyst for Steam Reforming of Dimethyl Ether by Metal (Fe, Zn or La) Addition for CO *in Situ* Removal

**Qi Zhang[1*], Yameng Chu[1], Xiaoqian Deng[1], Li Zhang[2], Hualong Chu[2]**

[1]Department of Chemical Engineering, East China University of Science and Technology, Shanghai, China
[2]State-Key Laboratory of Chemical Engineering, Department of Mechanical and Power Engineering, East China University of Science and Technology, Shanghai, China
Email: *zhangqi@ecust.edu.cn

**How to cite this paper:** Zhang, Q., Chu, Y.M., Deng, X.Q., Zhang, L. and Chu, H.L. (2018) Improvement of a Mesh-Type Cu/Ni/γ-Al2O3/Al Catalyst for Steam Reforming of Dimethyl Ether by Metal (Fe, Zn or La) Addition for CO *in Situ* Removal. *Modern Research in Catalysis*, **7**, 1-16.
https://doi.org/10.4236/mrc.2018.71001

**Received:** December 23, 2017
**Accepted:** January 28, 2018
**Published:** January 31, 2018



## Abstract

A mesh-type structured anodic alumina supported Cu/Ni bi-functional catalyst was developed for steam reforming of dimethyl ether (SRD). It was found that the Cu/Ni/γ-$Al_2O_3$/Al catalyst had remarkable catalytic activity and stability, but a high CO selectivity. Therefore, a multi-functional catalyst was proposed by metals (Fe, Zn, or La) addition to inhibit CO formation during the SRD process. The results show that promoter Fe can improve the Cu dispersion and decrease the reduction temperature of catalyst, and CO selectivity was minimized from 27% to around 3%. However, the addition of Zn and La only can decrease the CO selectivity to 12%. Furthermore, there was an excellent synergetic effect between Cu/Ni/γ-$Al_2O_3$ and Fe over the Cu/Ni/Fe/γ-$Al_2O_3$/Al catalyst by evaluating catalytic performance of catalysts with different packing structures. And the synergetic mechanism of the active components (γ-$Al_2O_3$, Cu or $Cu_2O$, and $Fe_3O_4$) for SRD and CO *in suit* removal was proposed. Finally, a 400-h durability test was carried out and the results show that the Cu/Ni/Fe/γ-$Al_2O_3$/Al catalyst had an excellent stability with a 100% DME conversion and low CO selectivity.

## Keywords

Anodic Alumina, Dimethyl Ether, Hydrogen, Fe Promoter, CO Removal

## 1. Introduction

As an alternative energy source, hydrogen has received much attention due to its

higher combustion efficiency, no-polluting characteristics and potential applications in several conversion processes. Moreover, it can be applied directly in transport and stationary power generation or via a hydrogenated intermediate ($H_2$ carrier) that can be transformed on-spot into $H_2$ by reforming for use in hydrogen fuel cells [1]. Compared with methanol, dimethyl ether (DME) is more suitable for being a $H_2$ carrier, since DME has higher energy density, non-corrosive and non-carcinogenic properties. Steam reforming of dimethyl ether (SRD) is proposed as a promising Hydrogen source for cell vehicles. The overall SRD proceeds via two successive steps: hydration of DME to methanol (MeOH) (Equation (1)), and methanol steam reforming to hydrogen (SRM) (Equation (2)).

DME hydrolysis:

$$CH_3OCH_3 + H_2O \rightarrow 2CH_3OH \Delta Hr = +37\ kJ \cdot mol^{-1} \quad (1)$$

MeOH steam reforming (SRM):

$$CH_3OH + H_2O \rightarrow 3H_2 + CO_2 \Delta Hr = +49\ kJ \cdot mol^{-1} \quad (2)$$

DME steam reforming (SRD):

$$CH_3OCH_3 + 3H_2O \rightarrow 6H_2 + 2CO_2 \Delta Hr = +135\ kJ \cdot mol^{-1} \quad (3)$$

It is generally acknowledged that DME hydrolysis to methanol proceeds over a solid acid catalyst, such as HZSM-5, H-mordenite, $ZrO_2$, and $\gamma$-$Al_2O_3$ [2]-[6]. Amongst them, $\gamma$-$Al_2O_3$ shows a higher catalytic stability along with the inhibition of side-reactions in DME hydrolysis, but its active temperature for DME hydrolysis ranges from 300˚C to 400˚C [7]. Meanwhile, SRM to produce hydrogen takes place over metal catalysts, in which Cu-based catalyst is the most widely applied due to its high activity and low price [8]. But the sintering of metallic Cu will lead to a poor thermal stability above 300˚C, which is a shortcoming for combining metallic Cu and $\gamma$-$Al_2O_3$ as the bi-functional catalysts for SRD. To solve this problem, copper-based spinel type of catalysts have been investigated as alternative metallic components, since they have a high thermal stability in SRD above 325˚C, but a very high temperature (up to 1000˚C) was required to prepare the spinel [9] [10] [11]. Another promising method is to improve the dispersion of metal Cu on the support by adding an extra metal. Fan *et al.* [12] prepared the Cu-based catalysts with a high thermal stability of 180 h at 400˚C by adding nickel. But the concentration of by-product CO is very high (above 25%), which will deteriorate the performance of proton exchange membrane fuel cells (PEMFC), so reducing the CO content in the hydrogen fuel is essential. Until now, there are two solutions proposed to address this problem. The first solution is the preferential oxidation (CO-PrOx) reaction with Fe-based catalyst follows the SRD stage to remove CO from hydrogen-rich gas. Yan *et al.* [13] decreased the CO concentration to 3% - 5% in the new-type SRD-COPrOx system by using a Pt/Fe-$\gamma$-$Al_2O_3$ catalyst, and the high temperature water gas shift reaction (HT-WGSR) was performed at 350˚C - 450˚C. However, the addition of extra reaction device will lead to the problem of the technical complexity and multiple stages. Second, the rare earth elements (lanthanum, La, etc.) have

been extensively applied to Ce-based materials to eliminate CO [14] [15]. Lu *et al.* [16] found that the addition of lanthanum into the Ni-based catalyst only decreased the CO selectivity to 23% from 35%. Therefore, the improvement of a multi-functional catalyst for SRD and the CO in situ removal is a new challenge, which can inhibit CO formation without any extra CO removal device.

Meanwhile, a structured anodic alumina catalyst was proposed due to its excellent flexibility and heat endurance, which is very promising in the application of micro-reactor [17] [18]. Differ to the conventional coating method, the anodic γ-$Al_2O_3$ layer on-situ generates from the surface of the aluminum substrate by anodization method. In our previous work, the generation mechanism and properties of the anodic alumina by different treatments were investigated [5] [6] [19].

In this study, a mesh-type Cu/Ni/γ-$Al_2O_3$/Al catalyst was prepared and applied in SRD. Different composition (Fe, Zn, or La) was evaluated by adding to the Cu/Ni/γ-$Al_2O_3$/Al catalyst. The series of catalysts were characterized by using $N_2O$ pulse chemisorption, XRD, $H_2$-TPR and BET to analysis the effects of different promoters on the catalysts' metallic dispersion and crystallite size. Meanwhile, the catalytic activity evaluations were carried out to compare CO in situ removal performance over different catalysts. Furthermore, the effects of packing structures on the catalytic performance were investigated. Finally, a 400-h stability evaluation was carried out over the optimized Cu/Ni/Fe/γ-$Al_2O_3$/Al catalyst.

## 2. Experimental

### 2.1. Catalyst Preparation

The flow scheme of the preparation of multi-catalysts was shown in **Figure 1**. The structured γ-$Al_2O_3$/Al monolith was prepared by the anodization method. The Al mesh (1060, 99.6%) was pretreated in a 10 wt% sodium hydroxide solution for 4 min and a 10 wt% nitric acid solution for 2 min, followed by a flush with deionized water. Then the pretreated mesh was anodized in a 0.4 mol/L oxalic acid solution for 10 h with a current density of 25 A/$m^2$ at 20˚C. The resulting mesh with porous alumina layers was calcined in air at 350˚C for 1 h to remove the residual oxalic acid. Afterward, it was subjected to hot water treatment (HWT) in deionized water at 80˚C for 1 h. Finally, the obtained meshes were dried and calcined in air at 500˚C for 4 h.

With the anodic alumina substrate, a series of Cu/X/γ-$Al_2O_3$/Al (X = Ni, Zn, La or Fe) catalysts were prepared through impregnation method. The monolithic γ-$Al_2O_3$/Al substrates were impregnated in an aqueous solution of Cu (II) nitrate or X nitrate (X = Ni, Zn, La or Fe) under ambient conditions. The prepared catalyst was then dried naturally, and calcined in air at 500˚C for 4 h.

### 2.2. Catalyst Characterization

The surface morphology of catalysts was measured by a scanning electron microscope (JSM-6360LV, JEOL).

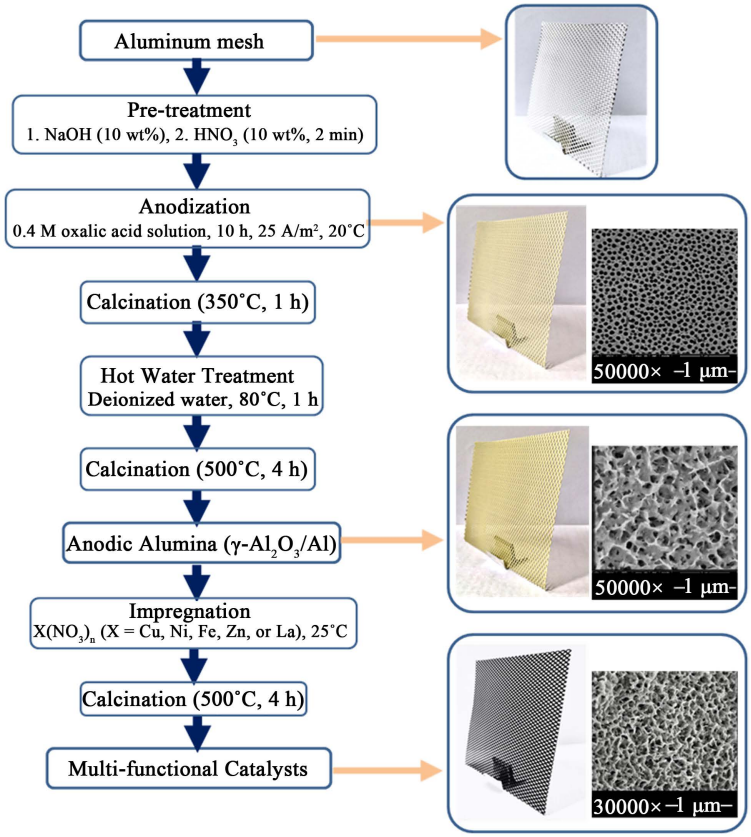


**Figure 1.** The flow schematic diagrams of the preparation of anodic alumina supported catalysts and photos (left) and SEM spectra (right) of catalysts with different steps.

The specific surface area and pore structure of catalysts was examined using adsorption method by a physisorption analyzer (ASAP 2020-M, Micromeritics). The specific surface area was calculated by the BET method, and the BJH method was used to determine the pore volume and average pore diameter.

The metal loading was analyzed by an Inductively Coupled Plasma-Atomic Emission Spectrometry (ICP-AES, 725ES, Agilent) and is reported here based on the quantity of the surface alumina layers.

An X-ray diffraction (D/max 2500 VB/PC, Rigaku) was applied to characterize the crystal structure of catalysts, and the average grain size of metal species was calculated through Scherrer's equation. The tested powder was scratched from the surface of the catalysts.

$H_2$ temperature-programmed reduction ($H_2$-TPR) analysis was performed in a Micromeritics ChemiSorb 2720 apparatus. Each sample including 100 mg catalyst was outgassed at 160˚C for 40 min under He flow (25 ml/min), then cooled to room temperature. Afterward, the temperature was raised to 920˚C with a ramping rate of 10˚C/min under a 10 vol% $H_2$/Ar flow atmosphere.

The dispersion of Cu and exposed copper surface area ($S_{Cu}$) were measured by selective $N_2O$ chemisorption method in a chemisorption analyzer (ChemiSorb 2720, Micromeritics). First, catalysts were reduced in a 10 vol% $H_2$/Ar stream at

400˚C for 2 h. Subsequently, the samples were purged with He at 400˚C for 20 min to remove hydrogen species adsorbed on the surface, and subsequently cooled to 50˚C. A flow of 20% $N_2O/N_2$ (30 mL/min) was used to oxidize surface copper atoms to $Cu_2O$ at 50˚C for 0.5 h. The reactor was flushed with He to remove the oxidant. Finally, another TPR experiment was performed in 10% $H_2$/Ar at a flow rate of 30 mL/min. The copper surface density is 1.46 × 1019 copper atoms per square meter. The copper dispersion (DCu) was defined as the ratio of copper atoms on the surface of the catalysts to the total amount of copper atoms in the catalyst.

X-ray photoelectron spectroscopy (XPS) was obtained with a Thermo ESCALAB 250 spectrometer with an Al Kα radiation. The binding energies scale (BEs) of the spectrometer was calibrated using the carbonaceous C 1s line at 284.6 eV.

### 2.3. Catalytic Activity and Durability Evaluation

Two different reactors were applied to quantify the catalytic performances of the catalysts under atmospheric pressure. The mesh-type catalysts were cut into small pieces (2 mm*2 mm), mixed with Raschig rings (20 - 40 mesh), then packed into a fixed-bed reactor (I.D. 12 mm). The catalyst charge was 3 g. And no $H_2$ pre-reduction treatment was conducted prior to the evaluation of catalysts. Figure 2 shows the diagram of the testing system for SRD. The water was injected with a constant flux pump and evaporated at 150˚C, then was mixed with DME and fed into the reforming chamber (fixed-bed reactor or microreactor). The compositions of reformate gases were determined by an on-line gas chromatograph equipped with a flame ionization detector (FID) and a thermal conductivity detector (TCD). The steam in the feed and reformate was trapped by a condenser before the gas analysis. A PORAPAK-Q column was used to separate the DME and $CH_4$ gas, and a TDX-01 column was used to separate the

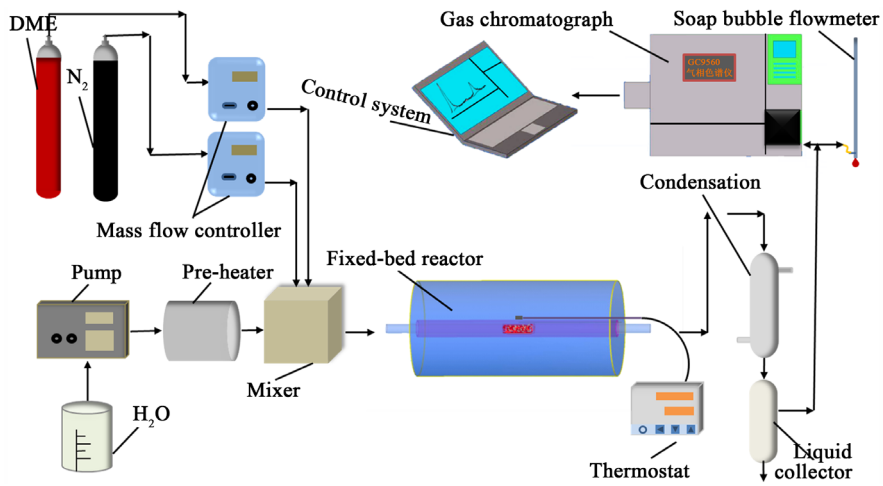


Figure 2. Schematic diagrams of the activity testing system for the DME reforming fixed-bed reactor to produce hydrogen.

CO, $CO_2$, and $N_2$. DME conversion and selectivity of products are defined as follows:

$$\text{DME conversion} = \frac{F_{DME,in} - F_{DME,out}}{F_{DME,out}} \times 100\% \quad (4)$$

$$\text{Selectivity of products} = \frac{F_{i,out}}{\sum F_{i,out}} \times 100\% \quad (5)$$

where $F_{DME,in}$ and $F_{DME,out}$ are the influent and effluent molar flow rates of DME, respectively, $F_{i,out}$ are the molar flow rates of gaseous products ($H_2$, CO, $CO_2$, $CH_4$).

## 3. Results and Discussion

### 3.1. Fe-, Zn- and La-Promoted Cu/Ni/γ-$Al_2O_3$/Al Catalysts Characterization

The chemical composition, surface area and pore properties of different catalysts were summarized in **Table 1**. It can be seen that the supporting material, γ-$Al_2O_3$/Al catalyst presented the highest BET surface area and pore volume. The addition of active metals decreased the specific surface and pore volume. This could be attributed to the deposition of the active components in pore and the block of micropore in the substrate. Besides, the Cu dispersion of different catalysts decreased in the order of: Cu/Ni/Fe/γ-$Al_2O_3$/Al > Cu/Ni/γ-$Al_2O_3$/Al > Cu/Ni/Zn/γ-$Al_2O_3$/Al > Cu/Ni/La/γ-$Al_2O_3$/Al, indicating that the Cu dispersion was improved by the incorporation of Fe promoter, while decreased by the addition of Zn or La.

In order to study the impacts of promoters on the crystal phases, the diffraction patterns for the Cu/Ni/γ-$Al_2O_3$/Al catalysts loaded with different metals were presented in **Figure 3(a)**. It can be seen that all four types of catalysts had strong peaks of CuO, which appeared at $2\theta = 35.6^\circ$ and $38.5^\circ$. Obviously, the addition of La and Zn promoters made the Cu diffraction peak sharper and stronger to varying degrees than Cu/Ni/γ-$Al_2O_3$/Al catalyst while the Cu/Ni/Fe/γ-$Al_2O_3$/Al catalyst exhibited the weakest peak of CuO. This further confirmed that the addition of Fe promoted the dispersion of Cu and reduced the crystallite size of Cu and Fe. The formation of smaller crystallite size of Cu provided more active sites, leading to more active catalyst at low temperature. There was no peak assigned to NiO, indicating that NiO existed in a high dispersion or a microcrystalline state on the gamma alumina substrate [20].

$H_2$-TPR was used to analyze the reduction properties of catalysts loaded with different metals. From **Figure 3(b)**, the two reduction peaks located at 425˚C and 750˚C for Fe/γ-$Al_2O_3$ were ascribed to the reduction of $Fe_2O_3$ to $Fe_3O_4$ and $Fe_3O_4$ to FeO or Fe, respectively [21] [22]. An interesting observation from this study was that the addition of Fe to Cu/Ni/γ-$Al_2O_3$/Al catalyst decreased the reduction temperature of hematite to magnetite considerably, to 259˚C. In general, the reduction temperature of CuO to Cu was around 300˚C [23]. For

**Table 1.** Physicochemical properties of the catalysts with different promoters.

| Catalyst | X loading[a] (wt%) | Cu loading[a] (wt%) | Ni loading[a] (wt%) | SBET ($m^2/g$) | Vp (mL/g) | Dp (nm) | $S^b_{Cu}$ ($m^2/g$) | $S^b_{Cu}$ (%) |
|---|---|---|---|---|---|---|---|---|
| $\gamma$-$Al_2O_3$/Al | - | - | - | 85 | 0.16 | 5.6 | - | - |
| Fe/$\gamma$-$Al_2O_3$/Al | Fe12.5 | - | - | 79 | 0.15 | 5.9 | - | - |
| Cu/Ni/$\gamma$-$Al_2O_3$/Al | - | 12.8 | 2.6 | 73 | 0.14 | 6.1 | 17.6 | 7.8 |
| Cu/Ni/Fe/$\gamma$-$Al_2O_3$/Al | Fe12.5 | 12.9 | 2.7 | 72 | 0.13 | 6.3 | 19.9 | 8.9 |
| Cu/Ni/Zn/$\gamma$-$Al_2O_3$/Al | Zn12.5 | 12.7 | 2.5 | 68 | 0.11 | 6.4 | 17.3 | 7.6 |
| Cu/Ni/La/$\gamma$-$Al_2O_3$/Al | La12.5 | 12.8 | 2.6 | 55 | 0.06 | 6.2 | 16.1 | 6.8 |

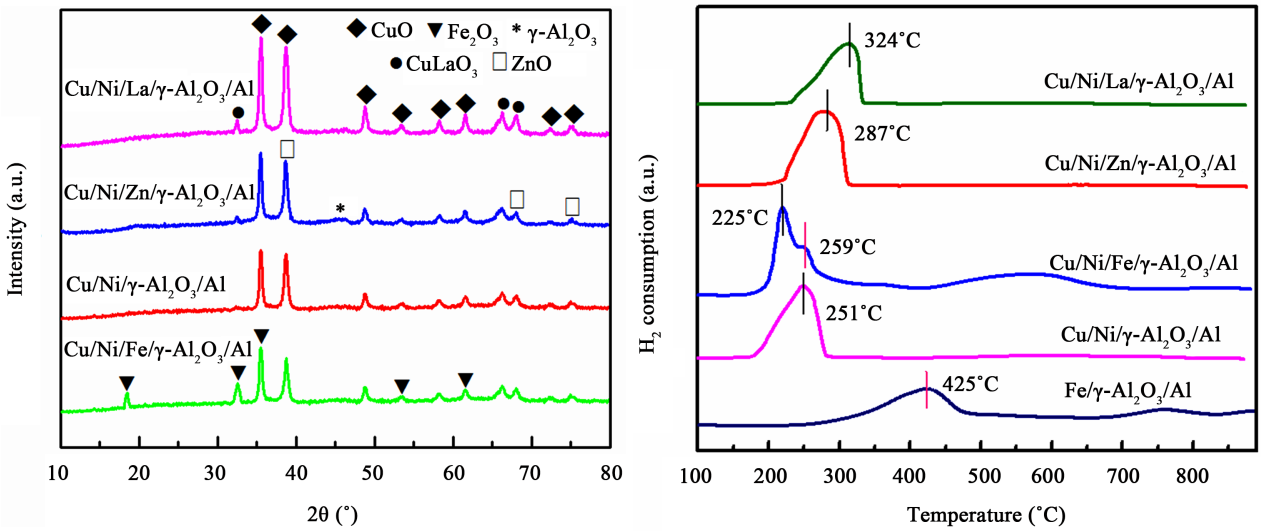


(a) (b)

**Figure 3.** (a) XRD patterns and (b) $H_2$-TPR profiles of $\gamma$-$Al_2O_3$ catalysts loaded with different metals.

Cu/Ni/Fe/$\gamma$-$Al_2O_3$/Al catalyst, the reduction peak of CuO decreased to 225˚C from 251˚C over the Cu/Ni/$\gamma$-$Al_2O_3$/Al catalyst. On the contrary, the addition of Zn and La to Cu/Ni/$\gamma$-$Al_2O_3$ made the reduction temperature increase to 287˚C and 324˚C, respectively. The results were consistent with Table 1 and XRD analysis, which indicated that compared with the Cu/Ni/$\gamma$-$Al_2O_3$ catalyst, a higher metallic dispersion and a decrease of the crystallite size lead to an improvement of reducibility for Cu/Ni/Fe/$\gamma$-$Al_2O_3$ catalyst.

### 3.2. Catalytic Behaviors of Fe-, Zn- and La-Promoted Cu/Ni/$\gamma$-$Al_2O_3$/Al Catalysts for CO *in Suit* Removal

Figure 4 shows the influences of promoters and temperatures on the values of the DME conversion and the effect of CO in situ removal in SRD system. It can be seen that the DME conversion increased while CO selectivity decreased over all the catalysts with the temperature increasing, because SRD is endothermic. The Cu/Ni/La/$\gamma$-$Al_2O_3$/Al catalyst had the lowest DME conversion and $H_2$ selectivity. It was due to the generation of $CuLaO_3$ co-oxide that occupied and

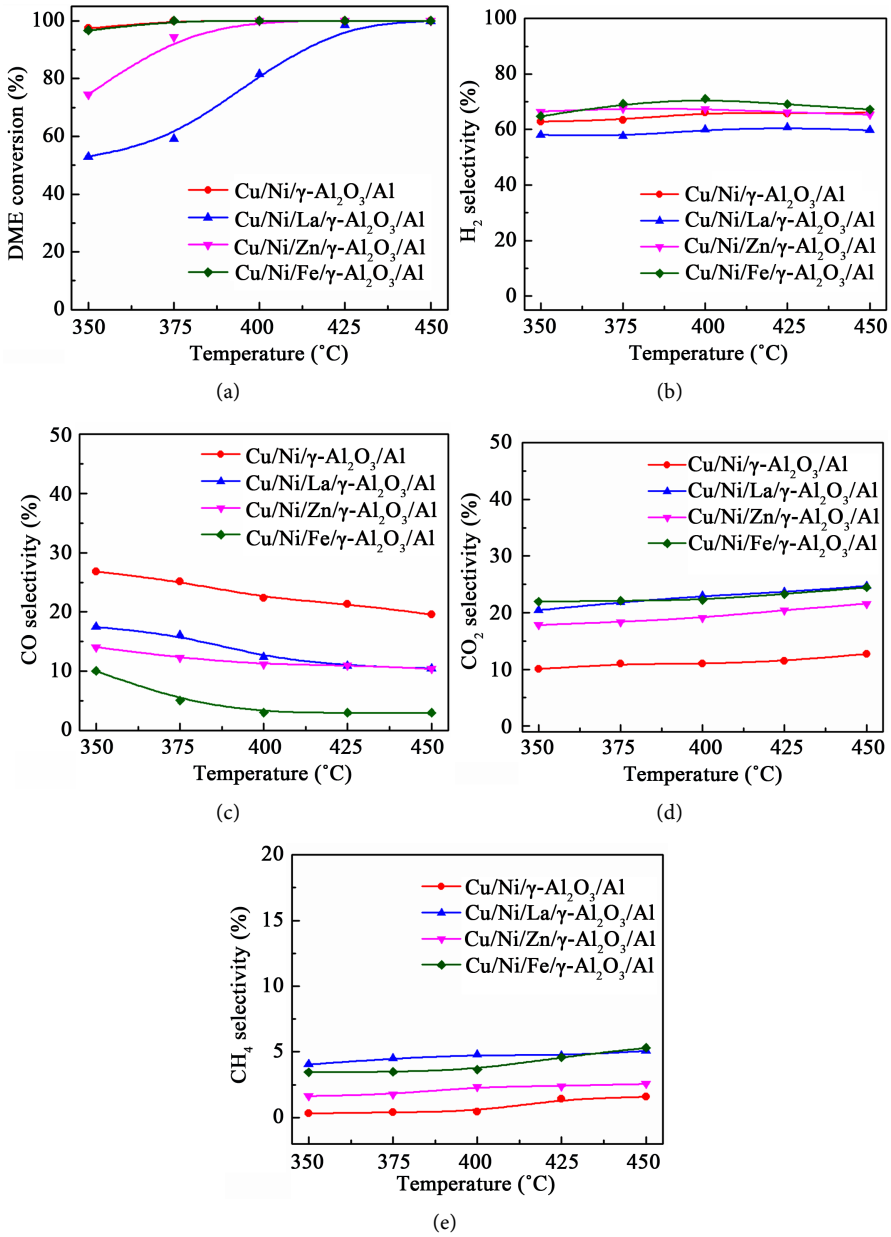


**Figure 4.** Catalytic performance of Cu/Ni/γ-$Al_2O_3$/Al catalysts with different metal loadings: (a) DME conversion; (b) $H_2$ selectivity; (c) CO selectivity; (d) $CO_2$ selectivity and (e) $CH_4$ selectivity; Reaction conditions: n(DME): n($H_2O$) = 1:4, Total flow rate = 4000 ml/(g·h).

decreased the active sites of Cu, and increased the reduction temperature of CuO. The Cu/Ni/Zn/γ-$Al_2O_3$/Al catalyst had a lower DME conversion than the Cu/Ni/γ-$Al_2O_3$/Al catalyst due to a lower dispersion of Cu (as shown in **Table 1**). As reported, Zn and La could promote WGSR (Equation (6)) and decrease the amount of CO [24] [25] [26] [27]. Nonetheless, the best temperature range is 250˚C - 300˚C for Cu/Zn/Al oxides [24], and 200˚C - 250˚C for $La_2O_3$/CuO/$CeO_2$ catalyst [26]. As such, the addition of Zn and La could not exhibit a better performance at the SRD reaction temperature at 350˚C - 450˚C. It also can be seen

that for the Cu/Ni/Fe/γ-$Al_2O_3$/Al catalyst performed the highest $H_2$ selectivity and best effect of CO removal. This was mainly attributed to that Fe-based catalysts have a high catalytic performance on WGSR (Equation (6)) above 330˚C [28] [29]. It was obvious that for Cu/Ni/γ-$Al_2O_3$/Al catalyst, the $H_2/CO_2$ molar ratio of ca. 6 was larger than that produced by the SRM process, indicating the step of methanol decomposition (Equation (7)) took place to produce $H_2$, and $CO_2$ methanation (Equation (9)) to consume $CO_2$. The fact that the selectivity of $CH_4$ increased with the decrease of CO selectivity indicated the occurrence of CO methanation (Equation (10)).

$$CO + H_2O \leftrightarrow CO_2 + H_2 \tag{6}$$

$$CH_3OH \rightarrow CO + 2H_2 \tag{7}$$

$$CH_3OCH_3 \rightarrow CH_4 + CO + H_2 \tag{8}$$

$$CO_2 + 4H_2 \leftrightarrow CH_4 + 2H_2O \tag{9}$$

$$CO + 3H_2 \leftrightarrow CH_4 + H_2O \tag{10}$$

### 3.3. The Synergetic Effect Behavior between Active Metals on the Cu/Ni/Fe/γ-$Al_2O_3$/Al Catalyst in the SRD

The catalytic performance of different packing structures of Fe/γ-$Al_2O_3$/Al and Cu/Ni/γ-$Al_2O_3$/Al was evaluated to investigate the synergetic effect between Cu/Ni/γ-$Al_2O_3$ and Fe on the Cu/Ni/Fe/γ-$Al_2O_3$/Al catalyst. The three packing structures included supported Cu/Ni/Fe/γ-$Al_2O_3$/Al catalyst, layered Cu/Ni/γ-$Al_2O_3$/Al (former) and Fe/γ-$Al_2O_3$/Al (later) and mechanical mixture of the two kinds of catalysts. For convenience, "supported Cu/Ni/Fe", "layered Cu/Ni+Fe" and "mixed Cu/Ni*Fe" represents above three packing structures, respectively. And "supported Cu/Ni" represents Cu/Ni/γ-$Al_2O_3$/Al. The results were showed in the **Figure 5**. It was found that DME conversion was 100% over the four catalysts above 375˚C. However, there was a large difference in the selectivity of $H_2$ and CO on different catalyst. The order of CO selectivity is: Cu/Ni > layered Cu/Ni+Fe > mixed Cu/Ni*Fe > supported Cu/Ni/Fe, while the $H_2$ selectivity had a contrary order. The minimum CO removal over layered Fe+Cu/Ni catalyst is mainly due to that WGSR over Fe/γ-$Al_2O_3$/Al can't proceed effectively after SRD over Cu/Ni/γ-$Al_2O_3$/Al, which results from the non-contact between the active components of Cu/Ni/γ-$Al_2O_3$ and Fe at the unit level. On the contrary, CO can be reformed to $CO_2$ and $H_2$ instantly over the supported Cu/Ni/Fe catalyst. This is probably because of the good synergetic effect of the active components of Cu/Ni/γ-$Al_2O_3$ and Fe at the atomic level.

To verify the change that occur in the oxidation of active components during SRD, XPS measurements were further performed on the Cu/Ni/Fe/γ-$Al_2O_3$ catalyst before and after above activity evaluation. "A-catalyst" and "B-catalyst" are used to represent the fresh and spent catalyst, respectively. The photoelectron peaks of the Cu 2p were presented in **Figure 6(a)**. It was found that the A-catalyst exhibited $Cu^+/Cu^0$ and $Cu^{2+}$ at near 932.4 and 934.4 eV, accompanied

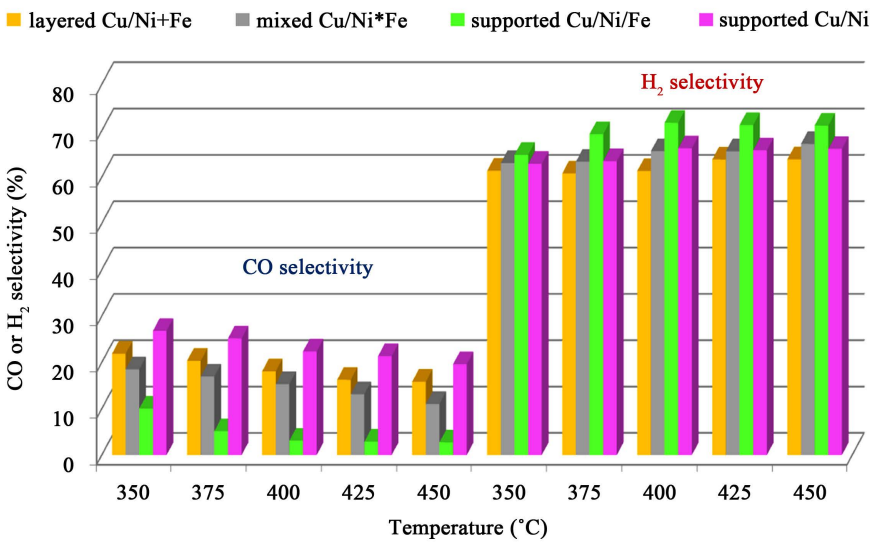


**Figure 5.** Catalytic performance of catalysts with different packing methods in SRD: $H_2$ selectivity and CO selectivity; Reaction conditions: n(DME): n($H_2O$) = 1:4, Total flow rate = 4000 ml/(g·h).

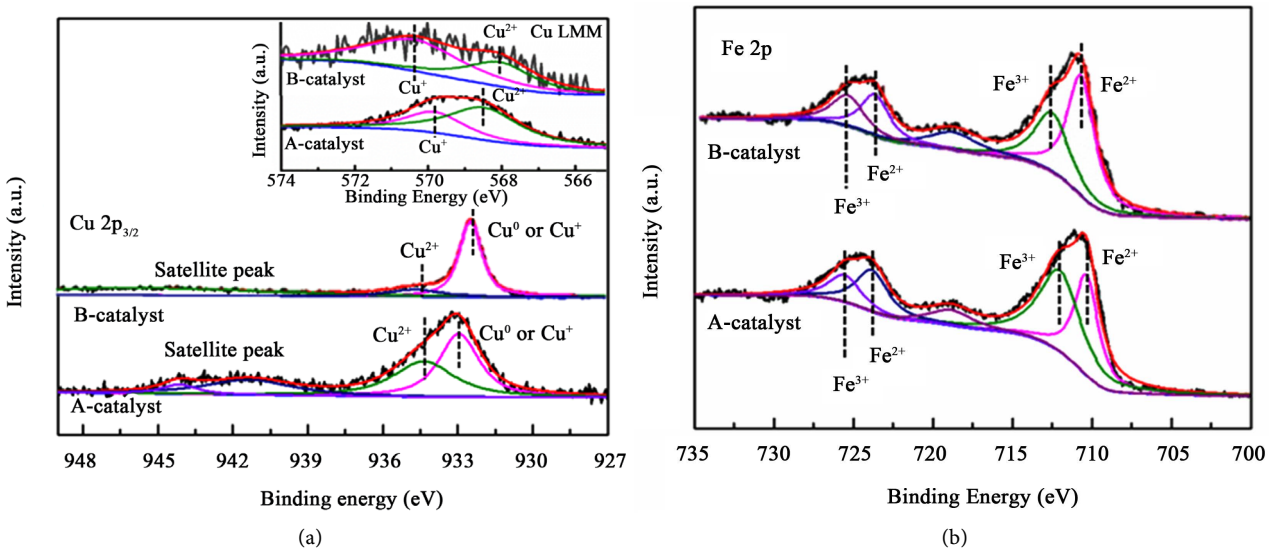


**Figure 6.** XPS spectra of Cu/Ni/Fe/γ-$Al_2O_3$/Al catalyst: (a) Cu $2p_{3/2}$ and Cu LMM (inset) XP spectra; (b) Fe 2p.

by the characteristic $Cu^{2+}$ shakeup satellite peaks (938 - 945 eV) [30] [31] [32]. B-catalyst exhibited the presence of $Cu^+/Cu^0$ at near 932.4 eV, along with a very slight amount of $Cu^{2+}$ species (satellite) at ca. 943 eV. Cu 2p3/2 XPS cannot be used to differentiate the peak at 932.4 eV between $Cu^+$ and $Cu^0$ species because they are separated by only 0.1 eV and neither would exhibit satellite peaks [33]. Auger Cu LMM spectra were used to verify the presence of $Cu^+$ at BE ~570 eV [33] [34]. Both the XPS and Cu LMM Auger spectra the $Cu^+/Cu^0$ and $Cu^{2+}$ species co-existed in the surface of A-catalyst. The surface compositions of the catalysts were calculated by measuring the areas under the curve, corresponding results were shown in Table 2. After evaluation, a significant increase from

**Table 2.** Surface composition estimated from XPS spectra.

| Catalyst | $Cu^0/Cu^+$ (%) | $Cu^{2+}$ (%) | $Fe^{2+}/Fe^{3+}$ |
|---|---|---|---|
| A-catalyst | 34.5 | 65.5 | 0.45 |
| B-catalyst | 91.1 | 8.9 | 1.12 |

34.5% to 91.1% in the amount corresponding to $Cu^+/Cu^0$ species was found. This observation confirms that the CuO species were reduced to metallic $Cu^+$ and $Cu^0$ species such as $Cu_2O$ and Cu, which further speculated the $Cu^+$ and $Cu^0$ species all are the active phase for the SRM process [35] [36].

The photoelectron peaks of the Fe 2p were presented in **Figure 6(b)**. The peaks of Fe 2p spectra were due to magnetite with contributions from both $Fe^{2+}$ and $Fe^{3+}$ ions. Specifically, $Fe^{2+}$ ions can be assigned to peaks around 710 ~ 711 eV with a satellite around 723 ~ 724 eV, while the peaks around 712 ~ 713 eV with a satellite at 725 ~ 726 eV are assigned to $Fe^{3+}$ ions [37] [38]. In was magnetite, 2/3 of the sites are occupied by $Fe^{3+}$ ions and 1/3 of the sites by $Fe^{2+}$ ions leading to a $Fe^{2+}/Fe^{3+}$ ratio in the bulk [37]. The results from **Table 2** showed that the $Fe^{2+}/Fe^{3+}$ fraction increased from 0.45 on the surface of the A-catalyst to 1.12 over B-catalyst, indicating that $Fe_2O_3$ and $Fe_3O_4$ species co-existed in the surface of A-catalyst, and $Fe_3O_4$ species existed in the surface of B-catalyst. The results further confirmed $Fe_3O_4$ supported active sites for WGS.

From the above XPS and catalytic performance results of Cu/Ni/Fe/γ-$Al_2O_3$ catalysts, the synergetic mechanism of the active components (γ-$Al_2O_3$, Cu or $Cu_2O$, $Fe_3O_4$) for SRD and CO in suit removal can be obtained in **Figure 7**. In the initial stage (**Figure 7(a)**), DME hydrolysis reaction took place on the γ-$Al_2O_3$/Al substrate to produce MeOH. Both DME and MeOH were decomposed to $CO_2$ and $H_2$ on $Cu_2O$ species. Meanwhile, the produced CO and reactant $H_2O$ were shifted to $CO_2$ and $H_2$ on $Fe_3O_4$ species with the WGSR. The produced $H_2$ initiated the reduction of the CuO and $Fe_2O_3$ to $Cu_2O$/Cu and $Fe_3O_4$ in turn. And the processes were recycled all the time until the CuO and $Fe_2O_3$ species on the catalyst could be completely reduced by hydrogen from SRD reaction. In the stabilization phase (**Figure 7(b)**), SRD was catalyzed on the γ-$Al_2O_3$/Al substrate and the reduced $Cu_2O$/Cu species, and then CO was directly transformed to $H_2$ and $CO_2$ on $Fe_3O_4$ specie.

### 3.4. Stability Evaluation of the Fe/Cu/Ni/γ-$Al_2O_3$/Al Catalyst

Since Cu/Ni/Fe/γ-$Al_2O_3$/Al catalyst had excellent catalytic performance, high $H_2$ selectivity, and low CO selectivity, it was selected to evaluate the thermal stability and the results were shown in **Figure 8**. It can be seen that Cu/Ni/Fe/γ-$Al_2O_3$/Al catalyst exhibited a good stability and no deactivation was observed during a 400 h test at 400˚C. And during the whole test process, DME conversion remained at 100%. The selectivity of $H_2$, $CO_2$ and $CH_4$ maintained at ca. 71.2%, 21.5% and 4.3%, while the CO selectivity remained at ca. 3.0%, which met the requirement of inlet CO concentration (3% - 5%) for HT-WGSR. In addition, the addition of

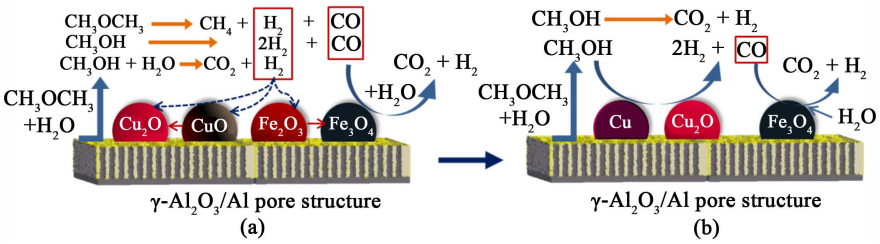


**Figure 7.** The synergetic mechanism of the active components over Cu/Ni/Fe/γ-$Al_2O_3$ for SRD and CO *in suit* removal: (a) initial stage; (b) stabilization stage.

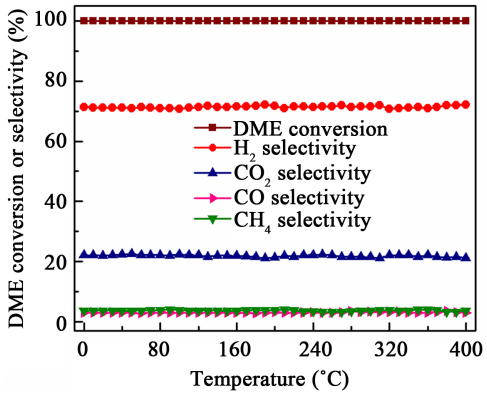


**Figure 8.** Stability test over the Cu/Ni/Fe/γ-$Al_2O_3$/Al catalyst, reaction conditions: n(DME): n($H_2O$) = 1:4, Total flow rate = 4000 ml/(g·h), T = 400˚C.

Fe to Cu/Ni/γ-$Al_2O_3$/Al catalysts not only promoted the in situ CO removal, but also reduced the crystallite size of Cu, thus improved the thermal stability of Cu/Ni/γ-$Al_2O_3$/Al catalyst.

## 4. Conclusions

The multifunctional Cu/Ni/γ-$Al_2O_3$/Al catalysts loaded with different metals were prepared to inhibit CO formation in SRD system. The conclusions based on the above experiments can be summarized as follows:

1) The Cu/Ni/γ-$Al_2O_3$/Al catalysts loaded different promoters (Fe, Zn or La) were investigated. It was found that Cu/Ni/Fe/γ-$Al_2O_3$ catalyst had the highest $H_2$ selectivity and the best CO *in situ* removal (from 27% to 3% CO selectivity). The characterization analysis showed that the Cu/Ni/Fe/γ-$Al_2O_3$ catalyst had the largest surface area and dispersion of Cu and the smallest Cu crystallite size. The WGSR was carried out over the $Fe_3O_4$ that had the similar optimized reaction range with SRD, which ensured the best reaction coupling effects.

2) The synergetic mechanism of the active components in SRD was obtained from the catalytic performance of catalysts with different packing structures and XPS analyses. It was evidenced that CO produced in SRD on $Cu_2O$ or Cu species can be reformed instantly to $CO_2$ and $H_2$ on $Fe_3O_4$ species. The $Cu_2O$ or Cu and the $Fe_3O_4$ species over Cu/Ni/Fe/γ-$Al_2O_3$/Al performed an excellent synergistic effect to enhance the CO *in situ* removal during the SRD.

3) The Cu/Ni/Fe/γ-$Al_2O_3$/Al catalyst exhibited an excellent stability in a 400-h durability test at 400˚C with a 100% DME conversion, a 71% $H_2$ selectivity and a 3% CO selectivity.

## Acknowledgements

This work was financially supported by the Fundamental Research Funds for the Central Universities (Grant No. 222201717013) and the Natural Science Foundation of Shanghai (Grant No. 16ZR1408200).

## References

[1] Qi, A., Peppley, B. and Karanet, K. (2007) Integrated Fuel Processors for Fuel Cell Application: A Review. *Fuel Processing Technology*, **88**, 3-22. https://doi.org/10.1016/j.fuproc.2006.05.007

[2] Lü, J.H., Zhou, S., Ma, K., Meng, M. and Tian, Y. (2015) The Effect of P Modification on The Acidity of Hzsm-5 And P-Hzsm-5/CuO-Zno-$Al_2O_3$ Mixed Catalysts for Hydrogen Production by Dimethyl Ether Steam Reforming. *Chinese Journal of Catalysis*, **36**, 1295-1303. https://doi.org/10.1016/S1872-2067(15)60883-X

[3] Matsumoto, T., Nishiguchi, T., Kanai, H., Utani, K., Matsumura, Y. and Imamura, S. (2004) Steam Reforming of Dimethyl Ether over H-Mordenite-Cu/$CeO_2$ Catalysts. *Applied Catalysis A: General*, **276**, 267-273. https://doi.org/10.1016/j.apcata.2004.08.013

[4] Ledesma, C. and Llorca, J. (2013) CuZn/$ZrO_2$ Catalytic Honeycombs for Dimethyl Ether Steam Reforming and Autothermal Reforming. *Fuel*, **104**, 711-716. https://doi.org/10.1016/j.fuel.2012.06.116

[5] Fan, F.Y., Zhang, Q., Xu, J.J., Ye, Q., Kameyama, H. and Zhu, Z.B. (2013) Catalytic Behavior Investigation of a Novel Anodized $Al_2O_3$/Al Monolith in Hydrolysis of Dimethyl Ether. *Catalysis Today*, **216**, 194-199. https://doi.org/10.1016/j.cattod.2013.07.013

[6] Zhang, Q., Sun, D.M., Fan, F.Y., Zhang, Q.H. and Zhu, Z.B. (2013) A Novel Monolith Catalyst of Plate-Type Anodic Alumina for the Hydrolysis of Dimethyl Ether. *Catalysis Communications*, **34**, 64-68. https://doi.org/10.1016/j.catcom.2013.01.016

[7] Semelsberger, T.A., Ott, K.C., Borup, R.L. and Greene, H.L. (2006) Generating Hydrogen-Rich Fuel-Cell Feeds from Dimethyl Ether (Dme) Using Physical Mixtures of a Commercial Cu/Zn/$Al_2O_3$ Catalyst and Several Solid-Acid Catalysts. *Applied catalysis B: Environmental*, **65**, 291-300. https://doi.org/10.1016/j.apcatb.2006.02.015

[8] Feng, D.M., Zuo, Y.Z., Wang, D.Z. and Wang, J.F. (2009) Steam Reforming of Dimethyl Ether over Coupled ZSM-5 and Cu-Zn-Based Catalysts. *Chinese Journal of Catalysis*, **30**, 223-229. https://doi.org/10.1016/S1872-2067(08)60098-4

[9] Oar-Arteta, L., Remiro, A., Vicente, J., Aguayo, A.T., Bilbao, J. and Gayubo, A.G. (2014) Stability of CuZnO$Al_2O_3$/HZSM-5 and $CuFe_2O_4$/HZSM-5 Catalysts in Dimethyl Ether Steam Reforming Operating in Reaction-Regeneration Cycles. *Fuel Processing Technology*, **126**, 145-154. https://doi.org/10.1016/j.fuproc.2014.04.028

[10] Shimoda, N., Muroyama, H., Matsui, T., Faungnawakij, K., Kikuchi, R. and Eguchi, K. (2011) Dimethyl Ether Steam Reforming under Daily Start-Up and Shut-Down (DSS)-Like Operation over $CuFe_2O_4$ Spinel and Alumina Composite Catalysts. *Applied Catalysis A: General*, **409-410**, 91-98. https://doi.org/10.1016/j.apcata.2011.09.031

[11] Faungnawakij, K., Shimoda, N., Fukunaga, T., Kikuchi, R. and Eguchi, K. (2008) Influence of Solid-Acid Catalysts on Steam Reforming and Hydrolysis of Dimethyl Ether for Hydrogen Production. *Applied Catalysis A: General*, **342**, 139-145. https://doi.org/10.1016/j.apcata.2008.02.039

[12] Fan, F.Y., Zhang, Q., Wang, X., Ni, Y.H., Wu, Y.Q. and Zhu, Z.B. (2016) A Structured Cu-Based/γ-$Al_2O_3$/Al Plate-Type Catalyst for Steam Reforming of Dimethyl Ether: Self-Activation Behavior Investigation and Stability Improvement. *Fuel*, **186**, 11-19. https://doi.org/10.1016/j.fuel.2016.08.036

[13] Yan, C.F., Hai, H., Guo, C.Q., Li, W.B., Huang, S.L. and Chen, H. (2014) Hydrogen Production by Steam Reforming of Dimethyl Ether and CO-PrOx in a Metal Foam Micro-Reactor. *International Journal Hydrogen Energy*, **39**, 10409-10416. https://doi.org/10.1016/j.ijhydene.2014.04.096

[14] Dong, F., Tanabe, T., Suda, A., Takahashi, N., Sobukawa, H. and Shinjoh, H. (2008) Investigation of the OSC Performance of Pt/$CeO_2$-$ZrO_2$-$Y_2O_3$ Catalysts by CO Oxidation and 18 O/16 O Isotopic Exchange Reaction. *Chemical Engineering Science*, **63**, 5020-5027. https://doi.org/10.1016/j.ces.2007.12.016

[15] Zhao, B., Wang, Q., Li, G. and Zhou, R.J. (2013) Effect of Rare Earth (La, Nd, Pr, Sm and Y) on the Performance of Pd/$Ce_{0.67}Zr_{0.33}$ $MO_{2-\delta}$ Three-Way Catalysts. *Journal of Environmental Chemical Engineering*, **1**, 534-543. https://doi.org/10.1016/j.jece.2013.06.018

[16] Lu, J.C., Li, X.F., He, S.F., Han, C.Y., Wan, G.P., Lei, Y.Q., Chen, R., Liu, P., Chen, K.Z., Zhang, L. and Luo, Y.M. (2017) Hydrogen Production via Methanol Steam Reforming over Ni-Based Catalysts: Influences of Lanthanum (La) Addition and Supports. *International Journal Hydrogen Energy*, **42**, 13647-3657. https://doi.org/10.1016/j.ijhydene.2016.08.165

[17] Zhang, Q., Zhu, X.D. and Kameyama, H. (2008) Numerical Investigations on the Development of Plate Reformers: Comparison of Different Assignments of the Chambers. *Aiche Journal*, **54**, 2707-2716. https://dx.doi.org/10.1002/aic.11592

[18] Zhang, L., Chu, H.L., Qu, H., Zhang, Q., Xu, H., Cao, J., Tang, Z.Y. and Xuan, J. (2018) An Investigation of Efficient Microstructured Reactor with Monolith Co/Anodic γ-$Al_2O_3$ Catalyst in Fischer-Tropsch Synthesis. *International Journal of Hydrogen Energy*, **43**, 3077-3086. https://doi.org/10.1016/j.ijhydene.2017.12.152

[19] Zhang, Q., Jiang, Z.R., Sun, D.M., Han, D.Y. and Zhu, Z.B. (2012) Effect of Crystalline State of Anodized Porous $Al_2O_3$/Al as Supports by Hydration. *Journal of Inorganic Materials*, **27**, 693-698.

[20] Jing, Q.S., Lou, H., Mo, L.Y., Fei, J.H. and Zheng, X.M. (2004) Combination of $CO_2$ Reforming and Partial Oxidation of Methane over Ni/BaO-$SiO_2$ Catalysts to Reduce Low $H_2$/CO Ratio Syngas Using A Fluidized Bed Reactor. *Journal of Molecular Catalysis A*: *Chemical*, **212**, 211-217. https://doi.org/10.1016/j.molcata.2003.10.041

[21] Liang, M.S., Kang, W.K. and Xie, K.C. (2009) Comparison of Reduction Behavior of $Fe_2O_3$, ZnO and $ZnFe_2O_4$ by TPR Technique. *Journal of Natural Gas Chemistry*, **18**, 110-113. https://doi.org/10.1016/S1003-9953(08)60073-0

[22] Khan, A., Chen, P., Boolchand, P. and Smirniotis, P.G. (2008) Modified Nano-Crystalline Ferrites for High-Temperature WGS Membrane Reactor Applications. *Journal of Catalysis*, **253**, 91-104. https://doi.org/10.1016/j.jcat.2007.10.018

[23] Ledesma, C. and Llorca, J. (2011) Dimethyl Ether Steam Reforming over Cu-Zn-Pd/$CeO_2$-$ZrO_2$ Catalytic Monoliths. The Role of Cu Species on Catalyst Stability. *The Journal of Physical Chemistry C*, **115**, 11624-11632. https://doi.org/10.1021/jp202044f

[24] Nishida, K., Li, D.L., Zhan, Y.Y., Shishido, T., Oumi, Y., Sano, T. and Takehira, K. (2009) Effective MgO Surface Doping of Cu/Zn/Al Oxides as Water-Gas Shift Catalysts. *Applied Clay Science*, **44**, 211-217. https://doi.org/10.1016/j.clay.2009.02.005

[25] Kam, R., Selomulya, C., Amal, R. and Scott. J. (2010) The Influence of La-Doping on the Activity and Stability of Cu/ZnO Catalyst for the Low-Temperature Water-Gas Shift Reaction. *Journal of Catalysis*, **273**, 73-81. https://doi.org/10.1016/j.jcat.2010.05.004

[26] Fang, X., Chen, C.Q., Lin, X.Y., She, Y.S., Zhang, Y.Y. and Zheng, Q. (2012) Effect of $La_2O_3$ on Microstructure and Catalytic Performance of $CuO/CeO_2$ Catalyst in Water-Gas Shift Reaction. *Chinese Journal of Catalysis*, **33**, 425-431. https://doi.org/10.1016/S1872-2067(11)60337-9

[27] Ali Reza, S.R., Maryam, B.K. and Ali Reza, R. (2011) Water Gas Shift Reaction over $Zn\text{-}Ni/SiO_2$ Catalyst Prepared from $[Zn(H_2O)_6]_2[Ni(NCS)_6]\cdot H_2O/SiO_2$ Precursor. *Journal of Molecular Catalysis A*: *Chemical*, **344**, 11-17. https://doi.org/10.1016/j.molcata.2011.04.010

[28] Jha, A., Jeong, D.-W., Shim, J.-O., Jang, W.-J., Lee, Y.-L., Rode, C.V. and Roh, H.-S. (2015) Hydrogen Production by the Water-Gas Shift Reaction Using $CuNi/Fe_2O_3$ Catalyst. *Catalysis Science & Technology*, **5**, 2752-2760. https://doi.org/10.1039/C5CY00173K

[29] Kim, W., Mohaideen, K.K., Seo, D.J. and Yoon, W.L. (2017) Methanol-Steam Reforming Reaction over Cu-Al-Based Catalysts Derived from Layered Double Hydroxides. *International Journal Hydrogen Energy*, **42**, 2081-2087. https://doi.org/10.1016/j.ijhydene.2016.11.014

[30] Severino, F., Brito, J.L., Laine, J., Fierro, J.L.G. and Agud, A.L. (1998) Nature of Copper Active Sites in the Carbon Monoxide Oxidation on $CuAl_2O_4$ and $CuCr_2O$-Spinel Type Catalysts. *Journal of Catalysis*, **177**, 82-95. https://doi.org/10.1006/jcat.1998.2094

[31] Deutsch, K.L. and Shanks, B.H. (2012) Active Species of Copper Chromite Catalyst in C-O Hydrogenolysis of 5-methylfurfuryl Alcohol. *Journal of Catalysis*, **285**, 235-241. https://doi.org/10.1016/j.jcat.2011.09.030

[32] Liu, P. and Hensen, E.J.M. (2013) Highly Efficient and Robust $Au/MgCuCr_2O$-Catalyst for Gas-Phase Oxidation of Ethanol to Acetaldehyde. *Journal of the American Chemical Society*, **135**, 14032-14035. https://doi.org/10.1021/ja406820f

[33] Platzman, I., Brener, R., Haick, H. and Tannenbaum, R. (2008) Oxidation of Polycrystalline Copper Thin Films at Ambient Conditions. *The Journal of Physical Chemistry C*, **112**, 1101-1108. https://doi.org/10.1021/jp076981k

[34] Ma, Y.F., Guan, G.Q., Hao, X.G., Zuo, Z.J., Huang, W., Phanthong, P., Kusakabed, K. and Abudula, A. (2014) Highly-Efficient Steam Reforming of Methanol over Copper Modified Molybdenum Carbide. *RSC Advance*, **4**, 44175-44184. https://doi.org/10.1039/C4RA05673F

[35] Faungnawakij, K., Shimoda, N., Fukunaga, T., Kikuchi, R. and Eguchi, K. (2009) Crystal Structure and Surface Species of $CuFe_2O$-Spinel Catalysts in Steam Reforming of Dimethyl Ether. *Applied Catalysis B*: *Environmental*, **92**, 341-350. https://doi.org/10.1016/j.apcatb.2009.08.013

[36] Pereira, A.L.C., Berrocal, G.J.P., Marchetti, S.G., Albornoz, A., de Souza, A.O. and do Carmo Rangel, M. (2008) A Comparison between the Precipitation and Impregnation Methods for Water Gas Shift Catalysts. *Journal of Molecular Catalysis A: Chemical*, **281**, 66-72. https://doi.org/10.1016/j.molcata.2007.07.042

[37] Reddy, G.K., Boolchand, P. and Smirniotis, P.G. (2012) Unexpected Behavior of Copper in Modified Ferrites during High Temperature WGS Reaction-Aspects of $Fe^{3+} \leftrightarrow Fe^{2+}$ Redox Chemistry from Mössbauer and XPS Studies. *Journal Physical and Chemistry C*, **116**, 11019-11031. https://doi.org/10.1021/jp301090d

[38] Reddy, G.K., Boolchand, P. and Smirniotis, P.G. (2011) Sulfur Tolerant Metal Doped Fe/Ce Catalysts for High Temperature WGS Reaction at Low Steam to CO Ratios—XPS and Mössbauer Spectroscopic Study. *Journal of Catalysis*, **282**, 258-269. https://doi.org/10.1016/j.jcat.2011.06.016